Fuel 345 (2023) 128263

Contents lists available at ScienceDirect

Fuel

journal homepage: www.elsevier.com/locate/fuel

Full length article

Entropy generation in an opposed-flow laminar non-premixed flame—Effects of using reduced and global chemical mechanisms for methane–air and syngas–air combustion

Simon J. Lorentzen, Ivar S. Ertesvåg *

Department of Energy and Process Engineering, Norwegian University of Science and Technology, Kolbjørn Hejes vei 1b, NO-7491 Trondheim, Norway

ARTICLE INFO

Keywords:
Entropy production
Second law
Diffusion flame
Components of entropy generation
Individual reactions
Heat release

ABSTRACT

The distribution of entropy generation is calculated with the aim of comparing second-law results for reduced and global mechanisms against a detailed mechanism. For methane, the DRM19 mechanism and a global, one-step irreversible mechanism are used for comparison with GRI3.0. For an equimolar CO/H_2 mixture, the Davis et al. mechanism and a global mechanism are compared with GRI3.0 for flames at 1, 10 and 20 atm. Conduction is the largest contributor to entropy generation, followed by mass diffusion and chemical reactions. For the conduction and mass-diffusion components, the reduced mechanisms give results close to the full mechanism. The global mechanisms have some deviations due to, among other things, inaccurate prediction of flame position and temperature. Overall, entropy generation by chemical reactions of the reduced mechanisms correspond to full mechanism reasonably well, in spite of larger deviations between the individual reactions included in both mechanisms. When reactions are left out in mechanism reduction, their effects are compensated by adjustments in the remaining reactions. These are clearly made with objectives other than entropy generation. Reaction-by-reaction comparison shows that the importance with respect to entropy generation can be very different to that of heat release. Some simplified models are also investigated.

1. Introduction

A large fraction of all energy conversion goes through chemical reactions. To improve and optimize such processes, the 2nd law has to be considered. Thus, enabling scientists and engineers to locate and quantify the entropy generation and exergy destruction in combustion devices will be important for efficient use of energy.

Entropy generation in laminar premixed flames in a diversity of configurations has been investigated in a multitude of studies, some of them reported by Salimath and Ertesvåg [1]. In most cases of these studies, the chemical reactions gave the largest contribution, both locally in the most active reaction zone and integrated through the flame. The second largest contribution was the conductive heat transfer, followed by mass diffusion. Viscous forces were usually found negligible with respect to entropy generation in flames. Radiation was often neglected, however, when included, found to be of minor direct importance.

Laminar, non-premixed flames have been investigated by several researchers, both single-phase flames and gaseous flames around evaporating fuel droplets. In most cases, however not all, the conductive heat transfer was shown to be the larger contributor.

Jet flames, where the fuel jet flowed into a confined air coflow, were investigated by Datta [2] and Stanciu et al. [3]. The fuel was methane in global, one-step, non-reversible mechanisms. Jet flames in quiescent air was studied by Nishida et al. [4]. For hydrogen, they used an 8-species/16-reactions mechanism, while for methane, GRI Mech 3.0 was used without nitrogen chemistry (32 species/186 reactions). Briones et al. [5] studied a lifted jet flame, that is, partially premixed, which propagated upstream and became an anchored stable non-premixed flame. The fuel was methane with addition of hydrogen, and the chemical mechanism used was GRI Mech 1.2. All these studies found that conductive heat transfer give the larger overall part of entropy generation. Chemical reactions had a significant, however much lesser, contribution. However, for the thin zone around the stoichiometric contour, the chemical reactions had the largest contribution.

For flames around evaporating fuel droplets in an air flow, Raghavan et al. [6] and Pope et al. [7] found heat conduction to be the largest contributor to entropy generation. It was closely followed by chemical reactions, while mass diffusion was less important.

Recently Zhang et al. [8] and Yan et al. [9] investigated entropy generation in sooting diffusion flames computationally. These studies

* Corresponding author.
E-mail address: Ivar.S.Ertesvag@ntnu.no (I.S. Ertesvåg).

https://doi.org/10.1016/j.fuel.2023.128263
Received 7 September 2022; Received in revised form 27 March 2023; Accepted 29 March 2023
Available online 3 April 2023

showed notable soot formation from ethylene flames. The soot effects on entropy generation were significant, particularly in the chemical-reactions component, but also in the mass-diffusion component.

Chen and co-workers [10,11] studied planar laminar counter-flow non-premixed flames of hydrogen, methane and hydrogen/methane mixtures against air, and also "MILD" conditions with CO_2 or H_2O as dilutant [12]. For the hydrogen-air flames computations, the chemical reactions gave the largest entropy generation, while for certain conditions of methane and methane/hydrogen the conduction gave as large contributions as the reactions. Mass diffusion/mixing had much lower entropy generation.

All cited studies agreed that the contribution of viscous dissipation was negligible, except in zones where the other components were very small.

In the present investigation, non-premixed, opposing-flow flames were studied. The configuration was symmetric around the common axis for the fuel and air inflows. The fuels were methane and syngas (equimolar CO and H_2). A quasi-1-dimensional model was used, providing results along the axis between the two opposing inlets. The paper was based on the master thesis work of the first author [13].

The primary aim of this study was to see how well reduced and global chemical mechanisms represent the entropy generation as compared with a full mechanism. The works cited above used one mechanism (full, reduced or global) and made conclusions without discussing the effects of this choice. A secondary aim was to see if the widely used reduced mechanisms concurred with a proposal of [14] using entropy generation as a criterion for mechanism reduction. The motivation for these research questions was that full chemical treatment is computationally demanding and often not necessary for a study of the energy conversion. In engineering practice, the full chemical treatment may not even be affordable. A third aim was to see the distribution of entropy generation among the different causes of entropy in opposed-flow non-premixed laminar flames.

In the following, the theory, models, numerical tools and cases are described in Sections 2 and 3. Next, results are presented and discussed in Section 4, before conclusions are made.

2. Theory and models

2.1. Flow, mass and energy

Following Kee et al. [15], the governing equations can be simplified to the following. For continuity,

$$\frac{d(\rho u)}{dx} + 2\rho V = 0, \tag{1}$$

axial and radial momentum,

$$\rho u\frac{du}{dx} = -\frac{dp}{dx} + \frac{4}{3}\frac{d}{dx}\left[\mu\frac{du}{dx} - \mu V\right] + 2\mu\frac{dV}{dx}, \tag{2}$$

$$\rho u\frac{dV}{dx} + \rho V^2 = -\Lambda + \frac{d}{dx}\left(\mu\frac{dV}{dx}\right), \tag{3}$$

energy,

$$\rho c_p u\frac{dT}{dx} = \frac{d}{dx}\left(\lambda\frac{dT}{dx}\right) - \sum_{i=1}^{N_s} J_i c_{p,i}\frac{dT}{dx} - \sum_{i=1}^{N_s} h_i W_i\dot{\omega}_i - \frac{d}{dx}q_{\text{rad}} + \Phi, \tag{4}$$

species mass,

$$\rho u\frac{dY_i}{dx} = -\frac{dJ_i}{dx} + W_i\dot{\omega}_i. \tag{5}$$

Here, x and r are the axial and radial coordinates, u and v are the velocity components in these directions, $V = v/r$, ρ is the mixture mass density, p is pressure, μ is the mixture viscosity, $\Lambda = (\partial p/\partial r)/r = \Lambda(x)$ is the radial-pressure-gradient eigenvalue, T is the temperature, c_p and $c_{p,i}$ are the mixture and individual species specific heats, respectively, and λ is the mixture conductivity. W_i, h_i and Y_i are, respectively, the molar mass, specific enthalpy and mass fraction of species i, and N_s is the number of species. q_{rad} is the radiation heat flux, and Φ is the viscous dissipation heat. J_i is the diffusive mass flux of species i in the axial direction, and $\dot{\omega}_i$ is the volumetric molar production rate of species i. The gases were assumed ideal.

For the 1-dimensional case, the viscous forces are seen in the momentum-component equations, Eqs. (2)–(3). The viscous dissipation heat, Eq. (4), can be expressed as [16],

$$\Phi = \mu\left(2\left(\frac{\partial u}{\partial x}\right)^2 + 2V^2 - \frac{2}{3}\left(\frac{\partial u}{\partial x} + V\right)^2\right). \tag{6}$$

This term was assumed small (cf. [16]) and neglected in the solution, however, evaluated from the results for verification.

The species mass flux in x direction, $J_i = \rho Y_i V_i$, can be expressed by the multi-component formulation of the mass diffusion velocity,

$$V_i = \frac{1}{X_i\overline{W}}\sum_{j\neq i}^{N_s} W_j D_{ij} d_j - \frac{D_i^T}{\rho Y_i}\frac{d\ln T}{dx}. \tag{7}$$

Here, X_i is the mole fraction, $\overline{W}$ is the mixture molar mass, D_{ij} is the diffusion coefficient of species i into species j, D_i^T is the thermo-diffusion (Soret) coefficient, and d_j is the diffusion driving force,

$$d_j = \frac{dX_j}{dx} + \left(X_j - Y_j\right)\frac{d}{dx}(\ln p). \tag{8}$$

It can be noted that thermo-diffusion and pressure diffusion were included in Eqs. (7)–(8), whereas the Dufour effect of heat transfer was neglected.

For radiation, the model by Liu and Rogg [17] was used in Eq. (4),

$$-\frac{dq_{\text{rad}}}{dx} = -2k_{\text{p}}\left(2\sigma T^4 - B_{\text{fu}} - B_{\text{ox}}\right), \tag{9}$$

where k_{p} denotes the Planck mean absorption coefficient, σ is the Stefan–Boltzmann constant, $B = \epsilon\sigma T^4$ with ϵ as the mean emissivity, while subscripts "fu" and "ox" denote the boundaries at the fuel and oxidizer inlets.

2.2. Chemical reactions

The volumetric production rate of species i by chemical reactions is expressed from

$$\dot{\omega}_i = \sum_{j=1}^{N_R}\nu_{ij}q_j, \tag{10}$$

where $\nu_{ij} = \nu''_{ij} - \nu'_{ij}$ are the stoichiometric coefficients of reaction j, N_R is the number of reactions, and the reaction progress is expressed from

$$q_j = k_{\text{f}j}\prod_{i=1}^{N_s}\left(\frac{\rho Y_i}{W_i}\right)^{\nu'_{ij}} - k_{\text{r}j}\prod_{i=1}^{N_s}\left(\frac{\rho Y_i}{W_i}\right)^{\nu''_{ij}}. \tag{11}$$

Here, $k_{\text{f}j} = A_j T^{\beta_j}\exp(-E_j/(R_u T))$ is the forward rate coefficient, with R_u as the universal gas constant and A_j, β_j and E_j as parameters specified by the reaction mechanism. The reverse rate coefficient is determined by $k_{\text{r}j} = k_{\text{f}j}/K_{\text{c}j}$, where $K_{\text{c}j}$ is the corresponding equilibrium constant.

The volumetric reaction heat release rate for reaction j is expressed as

$$Q_j = -\sum_{i=1}^{N_s} W_i h_i \nu_{ij} q_j, \tag{12}$$

and the total heat release rate from all reactions is the sum of the contributions, $Q = \sum_{j=1}^{N_R} Q_j$.

2.3. Entropy generation

The expressions for the volumetric entropy generation rate along the axis were found from the source terms of the entropy "transport" equation developed from the procedure described by, among others, Haase [18] and Bird et al. [16]. It was decomposed into effects of viscous forces,

$$\sigma_{\text{visc}} = \frac{\Phi}{T}, \tag{13}$$

conduction heat flux,

$$\sigma_{\text{cond}} = \frac{\lambda}{T^2}\left(\frac{dT}{dx}\right)^2, \tag{14}$$

mass diffusion,

$$\sigma_{\text{diff}} = \sum_{i=1}^{N_s}(-J_i)\left(\frac{1}{T}\frac{dh_i}{dx} - \frac{ds_i}{dx}\right), \tag{15}$$

chemical reaction j,

$$\sigma_{\text{chem},j} = -\frac{1}{T}\sum_{i=1}^{N_s} W_i g_i \nu_{ij} q_j, \tag{16}$$

and radiation,

$$\sigma_{\text{rad}} = \frac{-q_{\text{rad}}}{T^2}\cdot\frac{dT}{dx}. \tag{17}$$

In the last expression, $-q_{\text{rad}}$ is the flux from Eq. (9), while Φ in Eq. (13) is expressed by Eq. (6).

In Eqs. (15)–(16), h_i, s_i and $g_i = h_i - Ts_i$ are, respectively, the specific enthalpy, specific entropy and specific Gibbs function (free energy) for species i. For ideal gases, the parenthesis in Eq. (15) can be reformulated as

$$\left(\frac{1}{T}\frac{dh_i}{dx} - \frac{ds_i}{dx}\right) = \frac{R_u}{W_i}\frac{1}{p_i}\frac{dp_i}{dx} = \frac{R_u}{W_i}\left(\frac{1}{X_i}\frac{dX_i}{dx} + \frac{1}{p}\frac{dp}{dx}\right). \tag{18}$$

All chemical reactions summarize as $\sigma_{\text{chem}} = \sum_{j=1}^{N_R}\sigma_{\text{chem},j}$. The sum of all the contributions is the local total volumetric entropy generation rate,

$$\sigma = \sigma_{\text{visc}} + \sigma_{\text{cond}} + \sigma_{\text{diff}} + \sigma_{\text{chem}} + \sigma_{\text{rad}}. \tag{19}$$

3. Configuration, cases and chemical mechanisms

3.1. Boundary conditions

The cases for the diffusion flame will be specified by the conditions of the inflows at $x = 0$ and $x = L$, where L is the distance between the two nozzles.

The mass flux $\dot{m}'' = \rho u$, temperature and mass fractions of each inlet are specified.

3.2. Chemical mechanisms

For methane–air combustion, the full mechanism GRI Mech 3.0 [19] was used. It consists of 325 elementary two-way reactions and involves 53 species. The reduced mechanism DRM19 [20] was also applied. This mechanism was based on GRI Mech 1.2 [21], and involved 21 species (including inert N_2 and Ar) participating in 84 elementary, two-way reactions.

For comparison, a global mechanism by Westbrook and Dryer [22] was used. This is a one-step, one-way (irreversible) reaction of methane with oxygen, $CH_4 + 2O_2 \rightarrow CO_2 + 2H_2O$. The reaction progress (only forward) can be written as

$$q_1 = -A[\text{CH}_4]^a[\text{O}_2]^b \exp(-E_a/(R_u T)), \tag{20}$$

where the parameters $A = 6.7\cdot 10^{12}$, $a = 0.7$, $b = 0.8$ and $E_a = 48.4$ [22] (their Table 2, Set 3) were specified in the mechanism for units cm-s-mol-kcal-K.

GRI Mech 3.0 was used for syngas–air combustion, as well. In addition, a reduced mechanism (14 species, 38 elementary reactions), optimized for H_2/CO by Davis et al. [23], was used.

The (quasi-)global mechanism by Cuoci et al. [24] was based on a mechanism of Dryer and Westbrook [25]. The parameters had been adjusted, and a third reaction appeared to be added by [24]. The three one-way reactions were

$$\begin{aligned} &\text{CO} + 0.5\text{O}_2 \rightarrow \text{CO}_2,\\ &\text{CO}_2 \rightarrow \text{CO} + 0.5\text{O}_2,\\ &\text{H}_2 + 0.5\text{O}_2 \rightarrow \text{H}_2\text{O}. \end{aligned} \tag{21}$$

The corresponding reaction progresses (forward only) were ([24], their Table 4)

$$\begin{aligned} q_1 &= 2.30\cdot 10^{14}\exp(-31700/(R_u T))[\text{CO}][\text{H}_2\text{O}],\\ q_2 &= 4.45\cdot 10^{9}\exp(-41300/(R_u T))[\text{CO}_2],\\ q_3 &= 1.35\cdot 10^{11}\exp(-6900/(R_u T))[\text{H}_2]^{0.87}[\text{O}_2]^{1.10}. \end{aligned} \tag{22}$$

Here, the pre-exponential factors were transformed to ensure reaction rates in mol/(cm^3 s). In the following, this mechanism will be denoted "CFFR".

3.3. Cases

The fuel was either pure methane or an equimolar CO/H_2 mixture (syngas). Air was specified as 21% O_2 and 79% N_2, molar based.

The mass fluxes were set to 2 kg/(m^2 s) for air and 1 kg/(m^2 s) for fuel. This corresponded to overall equivalence ratios of 0.116 for methane and 0.435 for syngas. These choices gave approximately the same molar flows from the air and fuel inlets. Consequently, the flame zone was located near halfway between the nozzles.

For all cases, both inflows had temperature 300 K, and the distance L between the nozzles was 0.030 m. For each fuel, computations were made with the three mechanisms described above. The cases were run with pressures 1 atm (101 325 Pa), 10 atm and 20 atm.

The customary definition of strain rate,

$$a_s = \frac{2(-u_{\text{ox}})}{L}\left(1 + \frac{u_{\text{fu}}}{(-u_{\text{ox}})}\frac{\rho_{\text{fu}}^{1/2}}{\rho_{\text{ox}}^{1/2}}\right), \tag{23}$$

where subscripts "fu" and "ox" refer to the fuel and oxidizer inlets, gave values of 190 s^{-1} (methane) and 193 s^{-1} (syngas) for 1 atm, 19 s^{-1} for 10 atm and 9.7 s^{-1} for 20 atm.

3.4. Code and properties

The analyses were made with the open-source code Cantera [26]. The models described above were all implemented from before, except the global mechanisms.

The thermodynamic properties $c_{p,i}(T)$, $h_i(T)$, $s_i(T, p_{\text{ref}})$ were evaluated from the 7-parameter "NASA polynomials" with coefficients of McBride et al. [27]. Similarly, viscosity, conductivity and diffusivity were evaluated from polynomials [28].

It can be noted that Eq. (9) was implemented in Cantera for effects of CO_2 and H_2O. Effects of other species, e.g. CH_4 and CO, were however neglected.

For the adaptive grid refinement procedure [26], the criteria were set to ratio: 2; slope and curve: 0.2, with the exception of the global-mechanism methane case at 1 atm (slope and curve: 0.08). The criteria led to different number of points in the axial direction for different cases.

The solution to Eqs. (1)–(11) was provided by the Cantera solver, while postprocessing in own scripts was used to calculate the entropy generation terms, Eqs. (13)–(19).

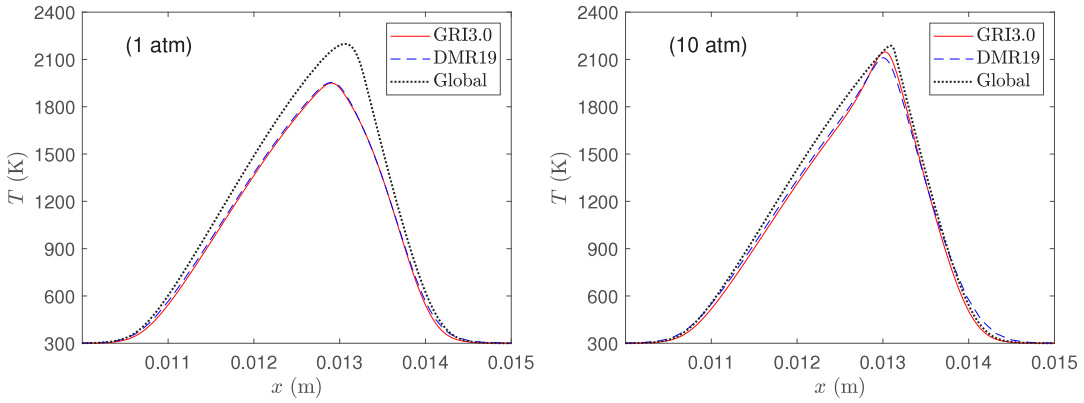

Fig. 1. Temperature along axis; methane–air, 1 atm and 10 atm.

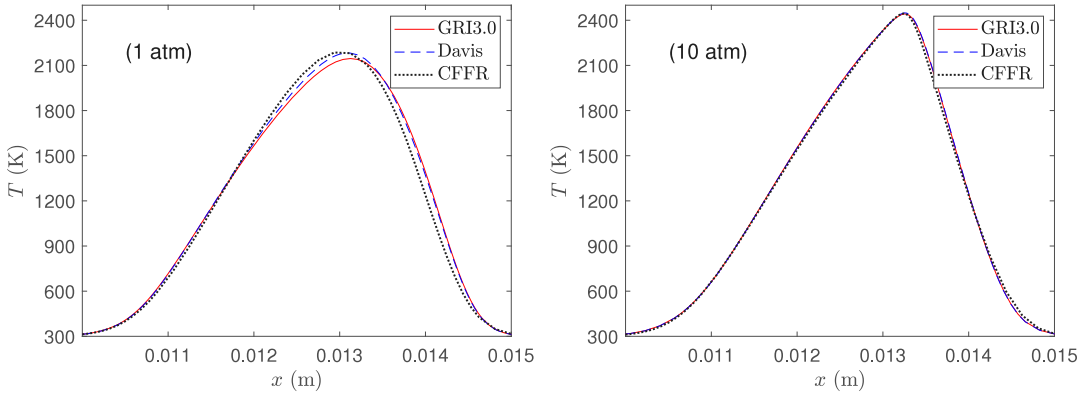

Fig. 2. Temperature along axis; syngas–air, 1 atm and 10 atm.

4. Results and discussion

4.1. Initial simulations, validation

The 1-dimensional model described above, Eqs. (1)–(5), was compared with a full 3-dimensional model by Luo et al. [29]. They found that the 1-dimensional model represented the flow quite well and "very similar" to the 3-dimensional model.

Som et al. [30] compared simulations to experiments of non-premixed counter-flow flames of syngas (50%/50% H_2/CO, molar based) and air. The temperature profile was "in close agreement" with experiments at atmospheric pressure, except for a shift of the position of the peak. This shift was explained by a strong suction to drain the effluents from the flame. The computational results of Som et al. at 1 atm (Fig. 2 of [30]) were well reproduced in the present study [13], both for GRI Mech 3.0 and the Davis et al. mechanism. Furthermore, the temperature profiles for 1, 5, 10, 15 and 20 atm (Fig. 8a of [30]) were well reproduced, using the same inflow conditions and the same mechanism (Davis et al.).

It was concluded that the code was verified and the model validated for further investigations of the opposed-flow flames.

4.2. Temperature and composition

The temperature of the methane–air cases at 1 atm and 10 atm are shown in Fig. 1. It was seen that for 1 atm, the global-mechanism peak temperature was higher than for the full and reduced mechanisms. It was also shifted a little towards the air inlet (to the right). The results for 20 atm were close to those of 10 atm and are not shown. Fig. 2 displays the corresponding results for syngas–air cases.

The mass fractions of CH_4, CO_2 and O_2 are shown in Fig. 3 for 1 atm and 10 atm with the full and the global mechanism. The results of the reduced mechanism (DRM19) were not visibly distinguishable from those of GRI 3.0, and are not included. The shift of the global-mechanism flame to the right (air inlet) is seen here, as well as in the CH_4 and O_2 profiles. The global mechanism converts all carbon to CO_2, while the detailed mechanisms include CO and other carbon compounds. Therefore, the CO_2 profile was higher for the global mechanism. The 10 atm and 20 atm results were similar, although with lesser differences between global and detailed mechanisms for CH_4 and O_2. This was consistent with the temperature results seen above. Fig. 4 shows the major species of the syngas–air flame at 1 atm and 10 atm. Again, the reduced mechanism (here, Davis et al.) did not deviate significantly from the full mechanism, and its results are not included.

The viscous dissipation heat, Φ (Eq. (6)), was neglected in the solution and evaluated from the results. In the flame (i.e. elevated temperature) the reaction heat release ranged from four to eighth orders of magnitude larger than the viscous term at 1 atm. Integrated through the flame, the ratio was $6 \cdot 10^6$. For higher pressures, the ratio was even larger.

4.3. Entropy generation components

This section will present results for entropy generation along the axis. Unless otherwise specified, all results here are entropy generation rates per unit of volume. The total entropy generation is shown in Fig. 5 for 1 atm and 10 atm for the three mechanisms of methane–air combustion. The 20 atm results were similar to those of 10 atm, except that the global and DRM19 peaks were relatively higher compared with the full mechanism. Fig. 6 shows the corresponding results for syngas.

Figs. 7 and 8 display the entropy generation due to conduction. This contribution followed the temperature gradient and provided distinct effects on both sides of the peak temperature. Results for 1 atm and 10

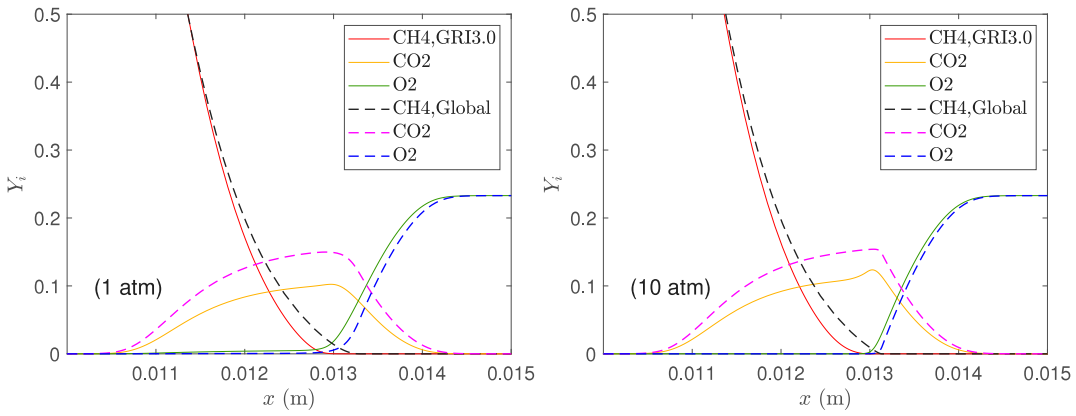

Fig. 3. Mass fractions of CH_4 (from left), CO_2 and O_2 (from right) along axis; methane–air, 1 atm and 10 atm, full mechanism and global mechanism.

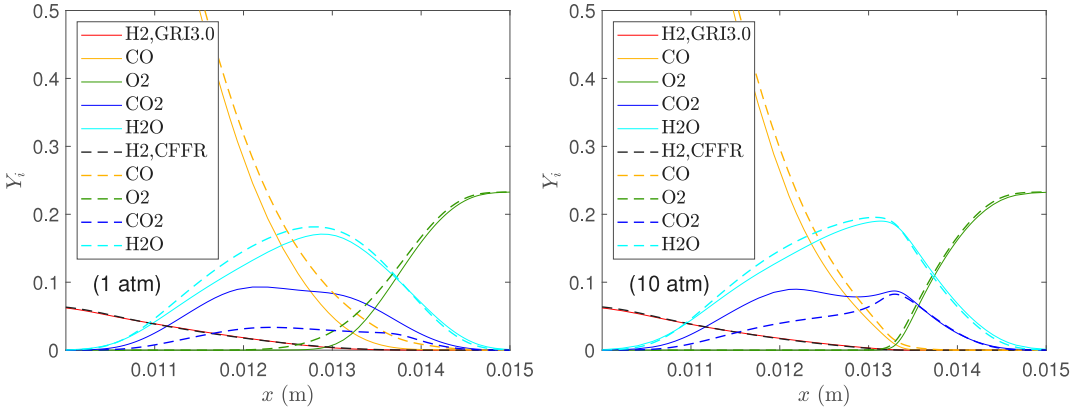

Fig. 4. Mass fractions of H_2 and CO (from left), O_2 (from right) CO_2 and H_2O along axis; syngas–air, 1 atm and 10 atm, full mechanism and global mechanism (CFFR).

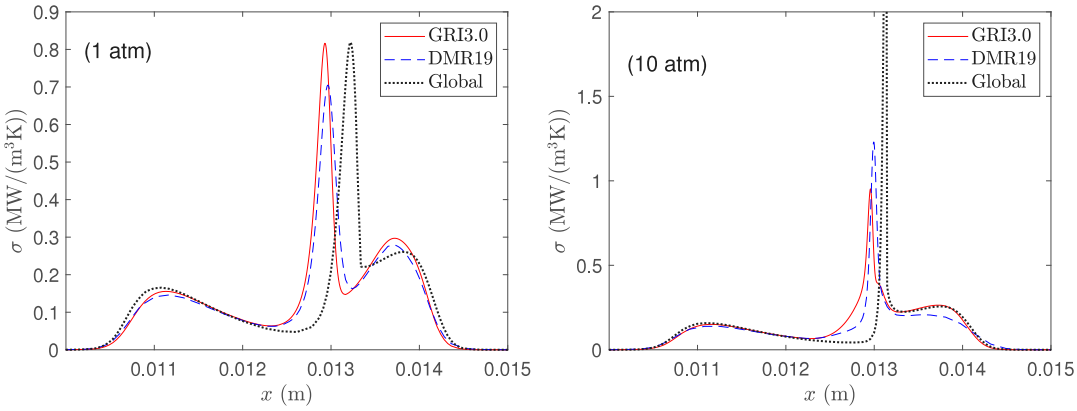

Fig. 5. Entropy generation along axis; methane–air, 1 atm and 10 atm.

atm are fairly similar to each other. Results for 20 atm had only minute differences from those of 10 atm and are not shown.

Mass diffusion entropy generation is shown in Figs. 9 and 10. The 20 atm results were narrower and with higher peaks for all mechanisms, otherwise similar to 10 atm.

Fig. 11 shows the entropy generation due to chemical reactions for methane. At 1 atm the results of the three mechanisms were close to each other, except for the shift in flame position for the global mechanism. The peaks for the reduced and global mechanisms became relatively higher for higher pressure (10 atm and 20 atm). The temperature and mass fraction profiles can partly, but hardly fully, explain the narrow spikes in the chemical entropy generation with the global mechanism. Hence, the reasons attribute to the mechanism itself. With no intermediates, the reactions take place in a narrower zone and with a shorter reaction timescale (faster completion of the reaction).

The syngas results are seen in Fig. 12. While methane had a primary peak slightly on the rich side of the peak temperature and a much lower secondary peak on the lean side, the situation was the opposite for syngas, with the dominating peak at the lean side. Furthermore, for increased pressure, the reduced syngas mechanism gave lower entropy generation than the full mechanism, contrary to the methane cases. For 10 atm, the quasi-global mechanism (CFFR) gave negative entropy generation besides the flame zone. This unphysical result seemed to be caused by a local imbalance between the heat releases of the individual reactions.

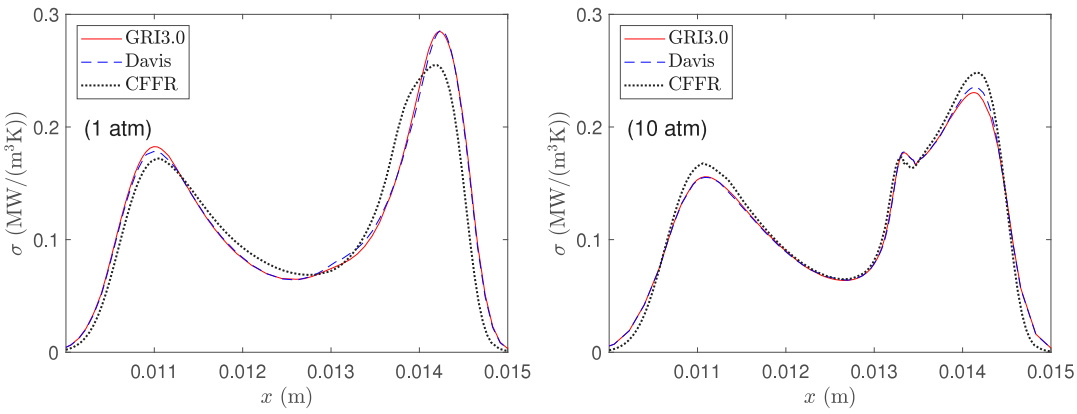

Fig. 6. Entropy generation along axis; syngas–air, 1 atm and 10 atm.

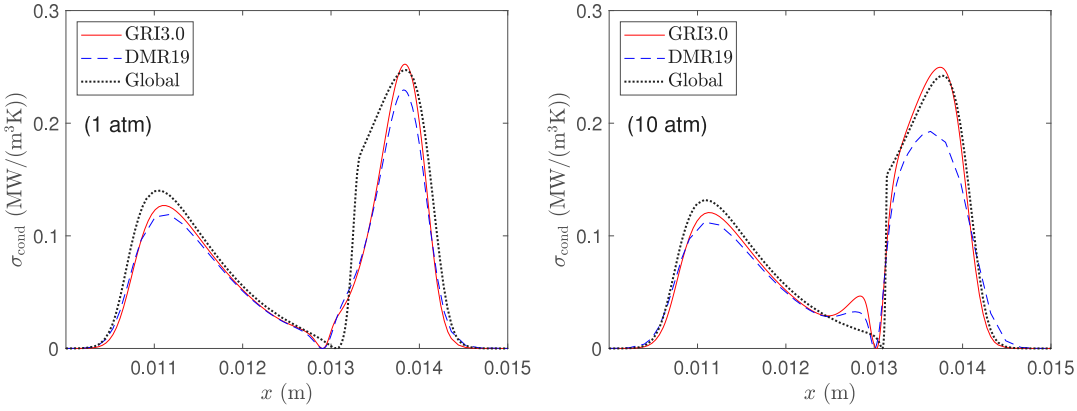

Fig. 7. Conduction entropy generation along axis; methane–air, 1 atm and 10 atm.

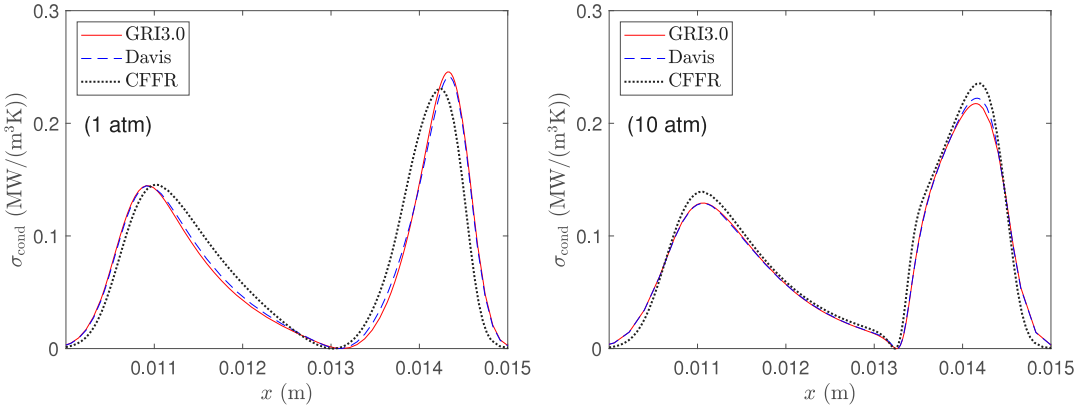

Fig. 8. Conduction entropy generation along axis; syngas–air, 1 atm and 10 atm.

Entropy generation due to viscous forces was five orders of magnitude less than the contributions shown above for 1 atm, and even smaller for 10 and 20 atm. The profiles are not shown here, but had two maxima corresponding to the maximum and minimum of the local strain rate. Close to the peak temperature, the strain rate and hence, the viscous entropy generation, had zero values.

The entropy generation due to radiation heat exchange was also very small compared to the major contributions, and the results are left out here. Its magnitude was four orders less than the major contributions for methane and six for syngas.

The volumetric total entropy generation rate and its components were integrated spatially along the axis, $\int_{x=0}^{L} \sigma dx$. The results are shown in Table 1, together with the integral of the volumetric reaction heat release rate. Also the peak temperature and its location is shown. For the reduced and global mechanisms, the integrated quantities and peak temperature are shown as relative deviations from the GRI 3.0 results.

It was seen that the reduced DRM19 mechanism for methane gave heat release rates and peak temperatures within minor deviations (2%) from the full mechanism. The conduction entropy generation is closely linked to the temperature, but had more notable deviations, particularly for the elevated pressure. For syngas the reduced-mechanisms results were close to those of the full mechanism, except for the (relatively small) chemical component of entropy generation.

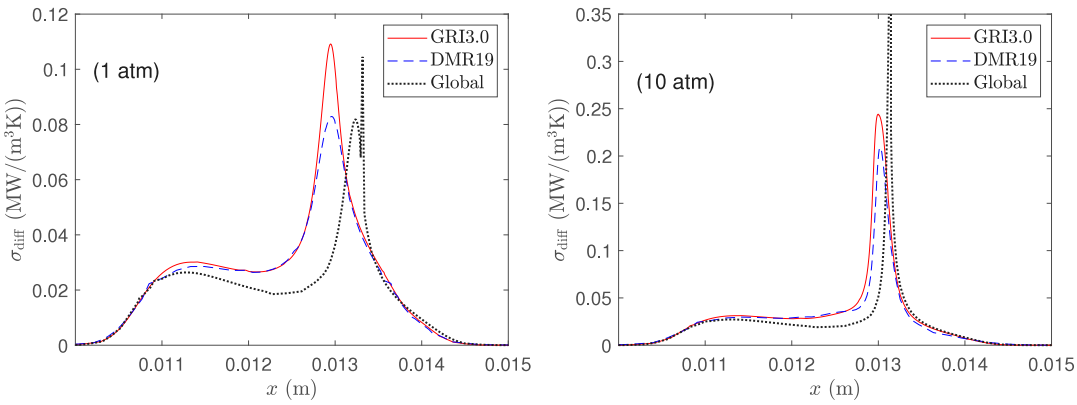

Fig. 9. Mass diffusion entropy generation along axis; methane–air, 1 atm and 10 atm.

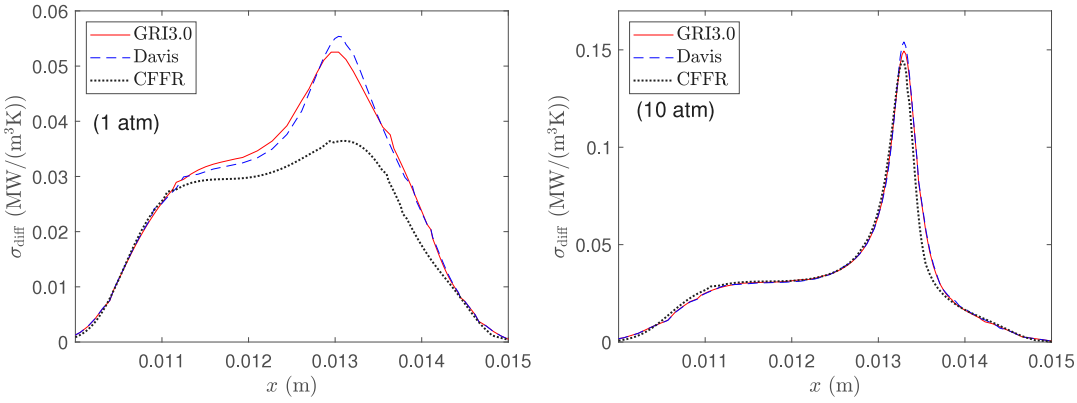

Fig. 10. Mass diffusion entropy generation along axis; syngas–air, 1 atm and 10 atm.

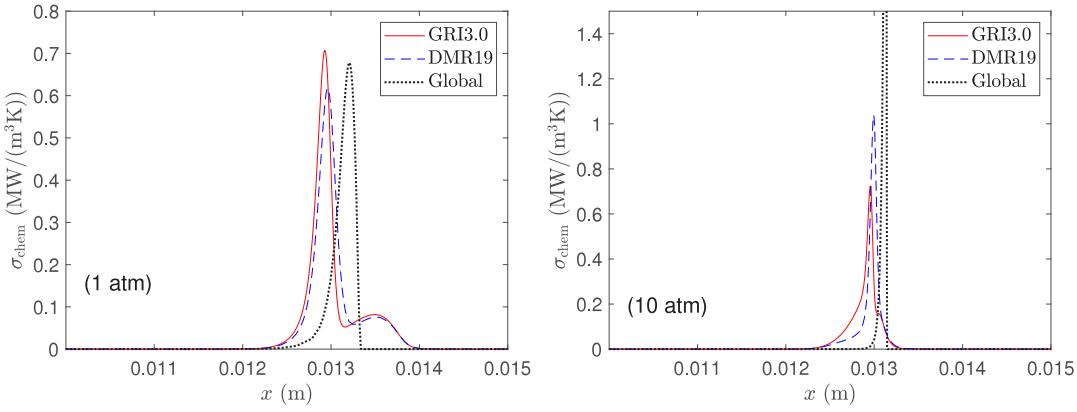

Fig. 11. Chemical reactions entropy generation along axis; methane–air, 1 atm and 10 atm.

4.4. Contributions to entropy generation by individual reactions

The total heat release for each location is the sum from all the elementary reactions, some positive (exothermic) and some negative (endothermic). To compare the impacts of the different reactions, the heat release rate (Eq. (12)) and its absolute value were both integrated along the axis between the nozzles. The latter integral was used to get a more appropriate view of both exo- and endothermic reactions, and in particular, for reactions that were endothermic at some locations and exothermic at other locations. Tables 2 and 3 show this integral as fractions of the integral of the net heat release rate. The sums of these fractions are above unity. For methane (1 atm) with GRI 3.0, the sum 1.8622 means that the endothermic contributions were −0.4311, and the exothermic 1.4311, times the net heat release rate. Furthermore, the entropy generation by each chemical reaction, Eq. (16), was also integrated along the axis. They are shown in the tables as fractions of the integrated total chemical reactions entropy generation rate.

The "Rank" shown in the tables indicates the importance of each reaction to the quantity in question. The first reaction in Table 2, $H+O_2 \rightleftharpoons O+OH$, was the most important for heat generation by both mechanisms. For entropy generation, however, it gave the 7th and 11th largest contributions with GRI 3.0 and DRM19, respectively.

It was seen that the important reactions for heat release in GRI 3.0 in these cases were also important in the reduced mechanisms (with $H + H_2O + O_2 \rightleftharpoons H_2O + HO_2$ as an exception). This observation was not equally clear for entropy generation. In particular, for methane, the most important GRI 3.0 reaction is not part of DRM19. This was compensated by other reactions, e.g., a reaction with low importance

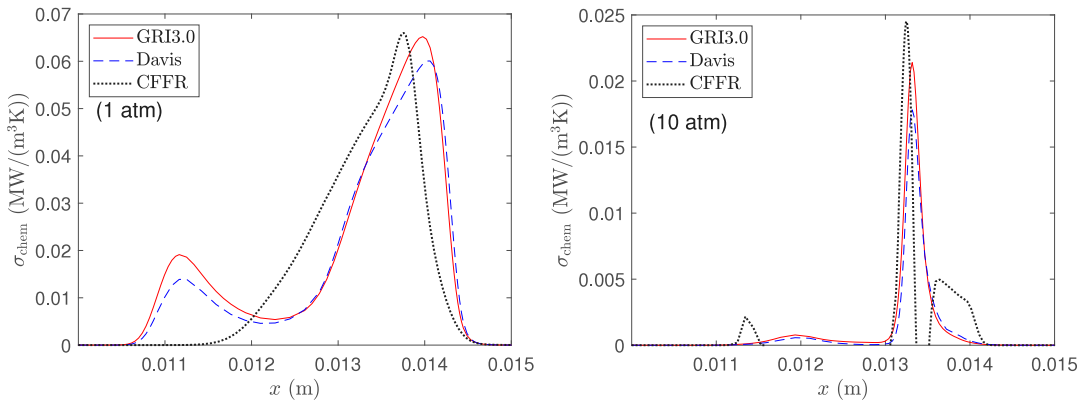

Fig. 12. Chemical reactions entropy generation along axis; syngas–air, 1 atm and 10 atm.

Table 1
Entropy generation rate and heat release rate integrated along the axis from nozzle to nozzle. Dimensional values for GRI 3.0, relative deviations for the other mechanisms. Peak temperature and its location.

Methane–air	GRI 3.0			DRM19			Global		
	1 atm	10 atm	20 atm	1 atm	10 atm	20 atm	1 atm	10 atm	20 atm
Conduction (W/(m^2 K))	323.5	364.4	357.1	−3.2%	−9.3%	−9.5%	18.6%	3.5%	1.0%
Diffusion (W/(m^2 K))	120.2	144.9	150.1	−5.8%	−10.6%	−12.6%	−22.2%	−21.2%	−23.2%
Chemical (W/(m^2 K))	209.2	128.9	123.8	−1.9%	2.6%	2.9%	−22.0%	6.0%	10.5%
Total (W/(m^2 K))	653.0	638.4	631.3	−3.2%	−7.2%	−7.7%	−1.9%	−1.5%	−2.7%
Heat release (kW/m^2)	379.4	385.9	387.0	2.0%	−1.5%	−1.6%	11.4%	3.2%	5.0%
Peak T (K)	1949.4	2147.6	2115.0	0.2%	−1.7%	−2.3%	12.8%	1.8%	−0.3%
Location (cm) of peak T	1.291	1.302	1.301	1.291	1.300	1.300	1.308	1.309	1.306
Syngas–air	GRI 3.0			Davis et al.			Global		
	1 atm	10 atm	20 atm	1 atm	10 atm	20 atm	1 atm	10 atm	20 atm
Conduction (W/(m^2 K))	361.2	400.5	389.6	1.0%	0.3%	−0.1%	4.1%	4.0%	4.3%
Diffusion (W/(m^2 K))	134.2	158.3	166.2	−0.4%	0.3%	0.3%	−17.2%	−2.2%	0.5%
Chemical (W/(m^2 K))	86.8	6.1	4.8	−6.4%	−16.6%	−21.2%	−11.6%	−33.6%	−45.4%
Total (W/(m^2 K))	582.3	565.3	561.2	−0.4%	0.2%	0.0%	−3.1%	1.8%	2.8%
Heat release (kW/m^2)	489.5	506.1	501.4	0.4%	0.0%	0.1%	−2.9%	−1.5%	−4.8%
Peak T (K)	2145.5	2441.6	2383.0	1.7%	0.3%	0.2%	2.3%	0.8%	0.8%
Location (cm) of peak T	1.313	1.325	1.324	1.308	1.325	1.325	1.303	1.323	1.324

(64th) in GRI 3.0 became the 2nd most important DRM19 reaction. A similar feature was seen in the syngas case: The 2nd most important GRI 3.0 reaction was missing, and compensated by other reactions.

The differences between heat and entropy contributions can be attributed to two features. First, the entropy generation is a function of the Gibbs energy difference, cf. Eq. (16), while heat release is a function of enthalpy difference, cf. Eq. (12). Second, dividing by temperature, Eq. (16), has a more pronounced effect for reactions taking place close to the peak temperature than for those important at lower temperatures.

The profiles of entropy generation rates for the 12 most important reactions in GRI 3.0 and in DRM19 are shown in Fig. 13 for the methane–air flame at 1 atm. It is seen that most reactions contributed in a range around the peak temperature (cf. Fig. 1) and summarized to the main peak seen in Fig. 11. However, some hydrogen/oxygen reactions contributed to the notable secondary peak on the lean side. Furthermore, reactions of hydrocarbons occurring mainly on the rich side widened the total profile, although without making another secondary peak.

The corresponding profiles are shown for syngas (1 atm) in Fig. 14. Here, one single reaction recombining radicals H and HCO was the dominating contributor to the peak on the rich side. Other important reactions contributed mainly to the lean-side peak in Fig. 12, which here had the primary peak.

The differences in weight of reactions between the full and the reduced mechanism are partly due to differences in reaction kinetics parameters (A_j, β_j, E_j), and partly due to differences in composition. In the methane–air flame, mass fractions of C_2H_4 and HCO had, respectively, 4.4 and 1.4 higher peak values with DRM19 compared with GRI 3.0. For CO, H_2, H and CH_2O this ratio was 0.7–0.9. For other species participating in the most important reactions, the peak values of DRM19 were close to those of GRI 3.0.

For elevated pressure, the temperature and species mass fraction profiles were not very different from 1 atm, Figs. 1–4. Therefore, the effects of pressure came mainly through the density in the reaction progress q_j, Eq. (11), cf. Eqs. (12) and (16), and through pressure dependent rate coefficients for some reactions. The changes in importance of elementary reactions were notable. For methane–air, the 12 most important reactions for entropy generation at 10 atm included only 5 from the list at 1 atm (rank 3, 11, 8, 7 and 6) for GRI 3.0. The reaction $CH_2O + H \rightleftharpoons H_2 + HCO$ increased from rank 3 at 1 atm to a fraction 0.0786 (integrated along the axis, cf. Table 2) and rank 1 at 10 atm, $CH_2O + OH \rightleftharpoons H_2O + HCO$ increased from rank 14 to rank 2 and fraction 0.0630, and $CH_2(s) + CO_2 \rightleftharpoons CH_2O + CO$ increased from rank 24 to rank 3 and fraction 0.0562. For DRM19, $C_2H_4 + O \rightleftharpoons CH_3 + HCO$ (fraction 0.2329), $CH_2(s) + CO_2 \rightleftharpoons CH_2O + CO$ (0.1144) and $CH_3 + O \rightleftharpoons CH_2O + H$ (0.0551) became the most important reactions for entropy generation at 10 atm. Here, the 12 most important reactions at 10 atm included 8 of the 12 most important at 1 atm.

4.5. Entropy generation as a criterion for mechanism reduction

Several entropy-generation studies were motivated by efficient energy conversion. Other studies have been seeking guidance to realizability of submodels. Among these can be regarded Kooshkbaghi

Table 2
Contributions (absolute values) relative to the total heat release rate and entropy generation rate from individual reactions integrated along the axis for methane, 1 atm, with GRI 3.0 and DRM19 mechanisms. "Rank" means the rank of importance for each quantity, and the included reactions are among the 25 most important for at least one of the quantities for one of the mechanisms. ("x": reaction not part of the mechanism).

Reaction	GRI 3.0				DRM19			
	Heat	Rank	Entropy	Rank	Heat	Rank	Entropy	Rank
$H + O_2 \rightleftharpoons O + OH$	0.1490	1	0.0353	7	0.1377	1	0.0335	11
$CH_3 + O \longrightarrow CO + H + H_2$	0.0439	14	0.0647	1	x	x	x	x
$CH_3 + O \rightleftharpoons CH_2O + H$	0.0666	6	0.0516	2	0.1268	2	0.1058	1
$H_2 + OH \rightleftharpoons H + H_2O$	0.1397	2	0.0073	40	0.1032	3	0.0059	32
$C_2H_4 + O \rightleftharpoons CH_3 + HCO$	0.0014	89	0.0022	64	0.0483	14	0.1001	2
$H + H_2O + O_2 \rightleftharpoons H_2O + HO_2$	0.1076	3	0.0444	4	0.0965	5	0.0399	7
$CH_2O + H \rightleftharpoons H_2 + HCO$	0.0333	20	0.0510	3	0.0300	23	0.0457	5
$CH_2 + O_2 \longrightarrow HCO + OH$	x	x	x	x	0.0620	9	0.0728	3
$CO + OH \rightleftharpoons CO_2 + H$	0.0916	4	0.0110	30	0.0960	6	0.0129	24
$CH_3 + H\ (+M) \rightleftharpoons CH_4\ (+M)$	0.0849	5	0.0087	36	0.0989	4	0.0115	26
$H_2O + HCO \rightleftharpoons CO + H + H_2O$	0.0335	19	0.0364	6	0.0508	11	0.0605	4
$H + HO_2 \rightleftharpoons 2\ OH$	0.0439	13	0.0396	5	0.0486	13	0.0444	6
$2\ CH_3\ (+M) \rightleftharpoons C_2H_6\ (+M)$	0.0580	7	0.0018	71	0.0658	7	0.0021	42
$C_2H_2 + H\ (+M) \rightleftharpoons C_2H_3\ (+M)$	0.0568	8	0.0215	16	x	x	x	x
$C_2H_4 + H\ (+M) \rightleftharpoons C_2H_5\ (+M)$	0.0527	9	0.0244	11	0.0643	8	0.0212	16
$HO_2 + OH \rightleftharpoons H_2O + O_2$	0.0457	12	0.0297	8	x	x	x	x
$HCO + M \rightleftharpoons CO + H + M$	0.0223	26	0.0242	12	0.0335	18	0.0399	8
$CH + H_2O \rightleftharpoons CH_2O + H$	0.0343	17	0.0258	9	x	x	x	x
$CH_2 + O_2 \longrightarrow CO + H + OH$	0.0088	42	0.0167	22	0.0178	29	0.0344	9
$H + N_2 + O_2 \rightleftharpoons HO_2 + N_2$	0.0499	10	0.0249	10	0.0459	16	0.0233	15
$HO_2 + OH \rightleftharpoons H_2O + O_2$	0.0484	11	0.0169	21	0.0549	10	0.0335	10
$CH_4 + OH \rightleftharpoons CH_3 + H_2O$	0.0407	16	0.0034	51	0.0490	12	0.0106	27
$CH_2O + OH \rightleftharpoons H_2O + HCO$	0.0280	23	0.0236	14	0.0348	17	0.0292	12
$CH + O_2 \rightleftharpoons HCO + O$	0.0227	25	0.0242	13	x	x	x	x
$CH_2(s) + CO_2 \rightleftharpoons CH_2O + CO$	0.0213	28	0.0160	24	0.0328	20	0.0265	13
$HO_2 + O \rightleftharpoons O_2 + OH$	0.0294	22	0.0231	15	0.0311	21	0.0246	14
$2\ OH \rightleftharpoons H_2O + O$	0.0414	15	0.0016	76	0.0300	22	0.0011	52
$CH_2 + CH_3 \rightleftharpoons C_2H_4 + H$	0.0278	24	0.0139	26	0.0467	15	0.0184	20
$C_2H_2 + O \rightleftharpoons H + HCCO$	0.0157	31	0.0199	17	x	x	x	x
$CH_2 + O \rightleftharpoons H + HCO$	0.0090	41	0.0077	37	0.0217	28	0.0192	17
$H + OH + M \rightleftharpoons H_2O + M$	0.0340	18	0.0112	29	0.0289	24	0.0098	28
$C_2H_2 + O \rightleftharpoons CH_2 + CO$	0.0214	27	0.0196	18	x	x	x	x
$H + HO_2 \rightleftharpoons H_2 + O_2$	0.0298	21	0.0167	23	0.0331	19	0.0188	18
$CH_2 + O_2 \longrightarrow CO_2 + 2\ H$	0.0141	33	0.0195	19	x	x	x	x
$CH_2 + OH \rightleftharpoons CH_2O + H$	0.0121	36	0.0077	38	0.0267	25	0.0184	19
$CH_4 + H \rightleftharpoons CH_3 + H_2$	0.0045	61	0.0182	20	0.0044	41	0.0168	22
$CH_2(s) + O_2 \rightleftharpoons CO + H + OH$	0.0057	54	0.0093	35	0.0104	33	0.0176	21
$H + HCO \rightleftharpoons CO + H_2$	0.0166	30	0.0074	39	0.0266	27	0.0132	23
$C + O_2 \rightleftharpoons CO + O$	0.0185	29	0.0139	25	x	x	x	x
$HCO + OH \rightleftharpoons CO + H_2O$	0.0123	35	0.0048	45	0.0266	26	0.0117	25
Other reactions	0.2847		0.2001		0.1282		0.0766	
Total	1.8622		1.0000		1.7117		1.0000	

et al. [14], who proposed a systematic procedure to reduce chemical mechanisms. The first step was to identify the reactions contributing at least a fraction ϵ (specified to 0.05) of the local instantaneous chemical entropy generation. They used this criterion for time instances of a transient homogeneous reactor. This would correspond to the locations along a 1-dimensional steady-state flame in the configuration here.

For the present case of methane–air (1 atm) with GRI 3.0, 44 reactions reached the criterion somewhere along the axis. Among these, 27 were found in DRM19. Within the range of x from 0.01209 m to 0.01404 m, where the chemical entropy generation was above 0.001 times its peak value (and visible in Fig. 11), only 20 reactions reached a local fraction of 0.05. Among these, 3 were not in DRM19 (and one not in GRI 1.2). Considering the 25 reactions that had the largest contributions when integrated along the axis (Table 2), 9 did not reach a local fraction of 0.05 anywhere. These 9 included the reactions with rank 9, 12 and 14 for entropy generation. Moreover, the reactions with the 2nd and 5th largest contributions to heat release, did not reach the criterion within the flame zone.

For the syngas case (1 atm) with GRI 3.0, 19 reactions had a local fraction at 0.05 or more. Only 8 of these were found in the Davis et al. reduced mechanism. For the range where local entropy generation reached above 0.001 of its peak value ($x = 0.01053 - 0.01474$ m), only 9 reactions had a local fraction of 0.05 or more. Five of these were found in the Davis et al. mechanism. Among the 20 most important reactions when integrated along the axis (Table 3), 7 satisfied the local 0.05 criterion. For instance, the reactions with rank 3, 6, 7 and 9 did not reach a local fraction of 0.05 anywhere.

It is kept in mind that although DRM19 was not derived from GRI 3.0, its starting point GRI 1.2 was closely related. Summarizing, it seems fair to state that neither DRM19 nor Davis et al. complied with the first criterion of the Kooshkbaghi et al. approach. The findings did not indicate that the approach would lead to better results for a reduced mechanism.

An issue still open for further research is to which extent an entropy-based approach for mechanism reduction, in general, will maintain key features like ignition delay and laminar flame speed. It is worth noting

Table 3
Contributions (absolute values) relative to total heat release rate and entropy generation rate from individual reactions integrated along the axis for syngas, 1 atm, with GRI 3.0 and Davis et al. mechanisms. For explanation, see Table 2.

Reaction	GRI 3.0				Davis et al.			
	Heat	Rank	Entropy	Rank	Heat	Rank	Entropy	Rank
$H_2 + OH \rightleftharpoons H + H_2O$	0.1816	1	0.0082	16	0.1628	2	0.0072	14
$H + OH + M \rightleftharpoons H_2O + M$	0.1810	2	0.1104	3	0.4359	1	0.2709	1
$H + HCO \rightleftharpoons CO + H_2$	0.0573	8	0.1634	1	0.0461	7	0.1309	3
$H + H_2O + O_2 \rightleftharpoons H_2O + HO_2$	0.1697	3	0.1550	2	x	x	x	x
$H + O_2 + M \rightleftharpoons HO_2 + M$	0.0089	19	0.0072	18	0.1281	4	0.1923	2
$H + O_2 \rightleftharpoons O + OH$	0.1293	5	0.0085	14	0.1340	3	0.0126	11
$HO_2 + OH \rightleftharpoons H_2O + O_2$	0.1303	4	0.0935	4	0.0881	5	0.0723	4
$H + HO_2 \rightleftharpoons 2\ OH$	0.0534	9	0.0919	5	0.0194	14	0.0418	8
$HO_2 + O \rightleftharpoons O_2 + OH$	0.0307	15	0.0565	8	0.0274	12	0.0612	5
$CO + OH \rightleftharpoons CO_2 + H$	0.0653	6	0.0085	15	0.0454	8	0.0058	16
$H + O + M \rightleftharpoons OH + M$	0.0029	26	0.0021	25	0.0648	6	0.0510	7
$HO_2 + OH \rightleftharpoons H_2O + O_2$	0.0587	7	0.0781	6	0.0436	9	0.0591	6
$H + N_2 + O_2 \rightleftharpoons HO_2 + N_2$	0.0506	10	0.0600	7	x	x	x	x
$H + HO_2 \rightleftharpoons H_2 + O_2$	0.0372	14	0.0409	9	x	x	x	x
$H_2O_2 + OH \rightleftharpoons H_2O + HO_2$	0.0284	16	0.0130	12	0.0184	15	0.0244	9
$2\ OH \rightleftharpoons H_2O + O$	0.0427	12	0.0010	28	0.0424	10	0.0011	25
$2\ H + H_2O \rightleftharpoons H_2 + H_2O$	0.0377	13	0.0314	10	0.0207	13	0.0159	10
$2\ OH\ (+M) \rightleftharpoons H_2O_2\ (+M)$	0.0452	11	0.0184	11	0.0316	11	0.0066	15
$2\ H + M \rightleftharpoons H_2 + M$	0.0139	17	0.0126	13	0.0143	17	0.0120	12
$H_2 + O_2 \rightleftharpoons H + HO_2$	x	x	x	x	0.0101	18	0.0109	13
$CO + OH \rightleftharpoons CO_2 + H$	x	x	x	x	0.0167	16	0.0034	18
$H + 2\ O_2 \rightleftharpoons HO_2 + O_2$	0.0055	22	0.0079	17	x	x	x	x
$CO + O\ (+\ M) \rightleftharpoons CO_2\ (+M)$	0.0082	20	0.0048	20	0.0065	20	0.0039	17
$H_2 + O \rightleftharpoons H + OH$	0.0105	18	0.0026	23	0.0083	19	0.0029	19
$2\ H + H_2 \rightleftharpoons 2\ H_2$	0.0044	24	0.0050	19	0.0023	23	0.0025	20
$HCO + M \rightleftharpoons CO + H + M$	0.0072	21	0.0033	22	0.0050	21	0.0023	21
$H + HO_2 \rightleftharpoons H_2O + O$	0.0036	25	0.0043	21	0.0013	25	0.0020	22
$H_2O + HCO \rightleftharpoons CO + H + H_2O$	0.0045	23	0.0014	26	0.0043	22	0.0013	24
$H + H_2O_2 \rightleftharpoons H_2O + OH$	0.0003	34	0.0004	33	0.0013	24	0.0018	23
$H + HCO\ (+M) \rightleftharpoons CH_2O\ (+M)$	0.0006	30	0.0022	24	x	x	x	x
Other reactions	0.0076		0.0074		0.0031		0.0040	
Total	1.3776		1.0000		1.3815		1.0000	

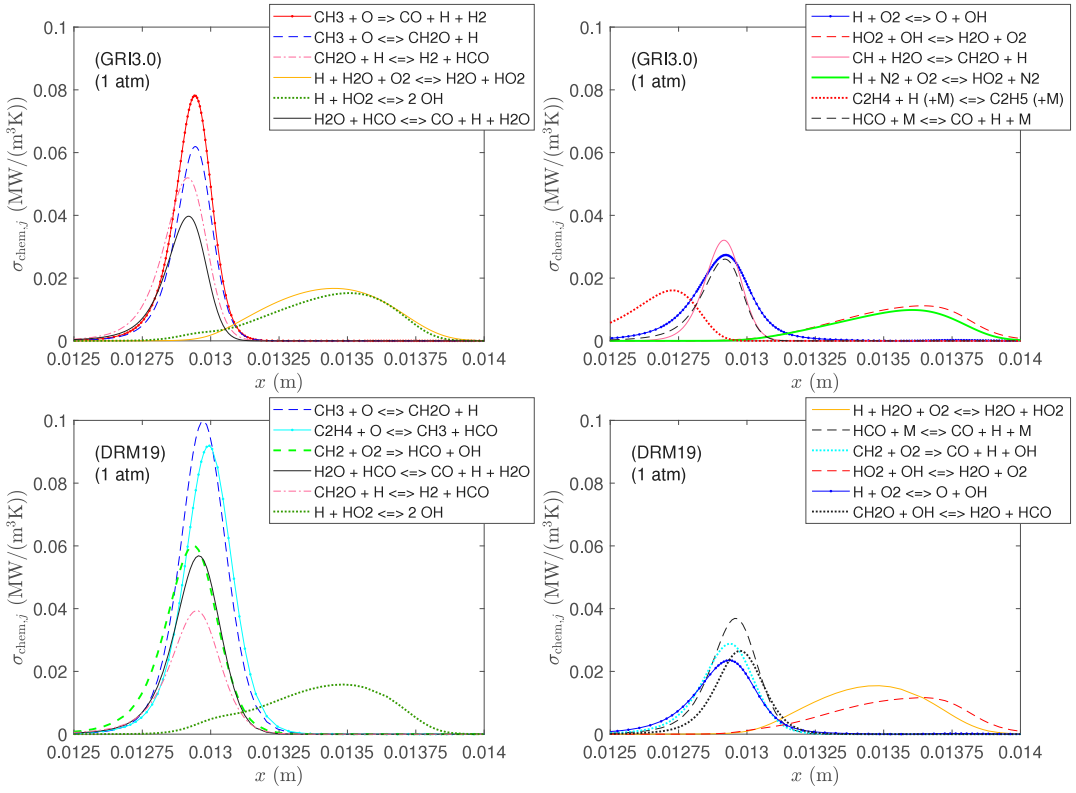

Fig. 13. Entropy generation along axis for 12 most important individual reactions; methane–air, 1 atm, GRI 3.0 and DRM19.

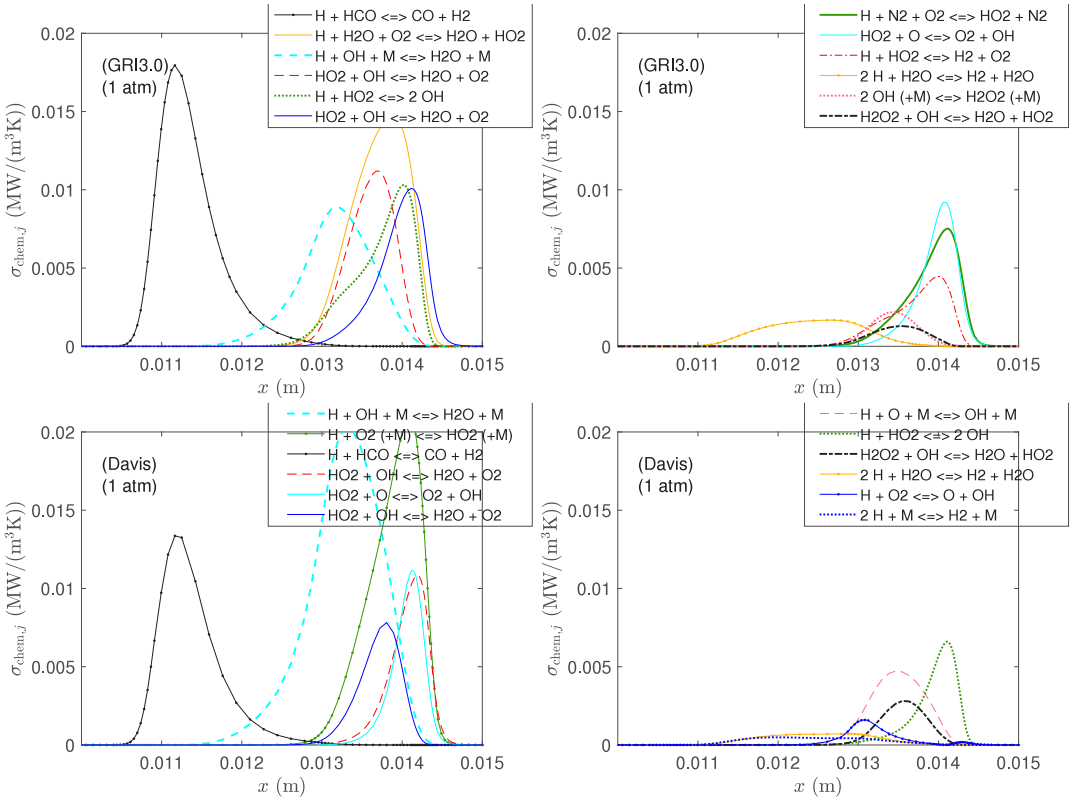

Fig. 14. Entropy generation along axis for 12 most important individual reactions; syngas–air, 1 atm, GRI 3.0 and Davis et al..

that said quantities depend, among other things, on heat release, which in a mechanism not necessarily corresponds to the entropy generation.

There is a small number of studies applying the referred method. Benekos et al. [31] used it providing a reduced mechanism (97 reactions, 20 species) for methane derived from GRI 3.0. This mechanism was tried for methane–air in the present work. Compared with GRI 3.0, the new mechanism gave slightly higher temperature (20–40 K on the rich side) for 1 atm, with a peak shifted slightly towards the air inlet. The chemical reactions entropy generation integrated through the flame was reduced by 2%, while the peak value was increased by 10%. The heat release rate increased by 2.5% integrated and its peak by 10%. The OH, O and H mass fraction peak values were reduced by 9%, 11% and 24%, respectively, while that of CO by 23%, although CO increased in the rich zone. The two reactions most important for entropy generation ($CH_3 + O \longrightarrow CO + H + H_2$ and $H_2 + OH \rightleftharpoons H + H_2O$, cf. Table 2) maintained their rank, while they increased their contributions by 80% (integrated) and peak values by 86%. The third and fourth increased by 7%–9%, while the 13th and 20th increased their contributions more than 3 times and became 3rd and 5th in rank. The mass-diffusion entropy generation integrated through the flame was reduced by 7% compared to the full GRI 3.0.

4.6. Simplified models for entropy generation

Some authors make use of simplified models for entropy generation. One approach is to calculate the chemical-reactions entropy generation as Q/T, where Q is the total reaction heat release rate (cf. Eq. (12)). For instance, Raghavan et al. [6] used this model in conjunction with a 1-step global reaction. For the present cases (1 atm), this model was compared to the full models of chemical-reaction entropy generation in Fig. 15. It was seen that for methane–air, the deviations due to the model were less than the deviations due to different chemical mechanisms. For syngas, the differences were much larger. This can primarily be explained by the distinction between the reaction enthalpy difference ($-\Delta H$) and the reaction Gibbs energy difference ($-\Delta G$) for the fuels in reaction with oxygen. The former is the heat release of the completed global reaction, while the latter divided by T represents the entropy generation of the same reaction (cf. Eq. (16)). For the temperature range of 1600–2100 K, the ratio of ($-\Delta G$) to ($-\Delta H$) for methane is very close to unity, approximately 0.99, whereas for H_2 and CO it is only 0.45–0.60.

Another approach (e.g. [32–34]) is simply to neglect all other contributions but viscous and conduction. For the present cases, the effects of this can be seen by comparing the conduction component, Figs. 7–8, with the total contribution, Figs. 5–6. The cited authors did not clearly argue in favour of the simplification, however, they referred sources dealing with non-reacting flows. For chemical reactions in equilibrium, the chemical reactions do not contribute to entropy generation. This is, however, not in general the case of conventional combustion. Indeed, the conduction appears to make the largest contribution to entropy generation in a diffusion flame, and it is located close to (although not in) the flame front. It gives an indication on the location and magnitude of the entropy generation. When this serves the aim of the investigation, neglecting all other contributions might make some sense.

4.7. Overall discussion

In the development of a detailed mechanism like GRI 3.0, a number of target data were used for comparison and optimization [19,35]. Although entropy and entropy generation were not among these target data, when heat release, temperature and species formation and transport are well captured, the entropy quantities should also be reasonably well predicted.

When it comes to reduced mechanisms, these are approximations to a more complete mechanisms, e.g. DRM19 [20] approximated GRI 1.2, and Davis et al. [23] was based on GRI 3.0. The reduction aimed at maintaining ignition delay and laminar flame speed, which rely on

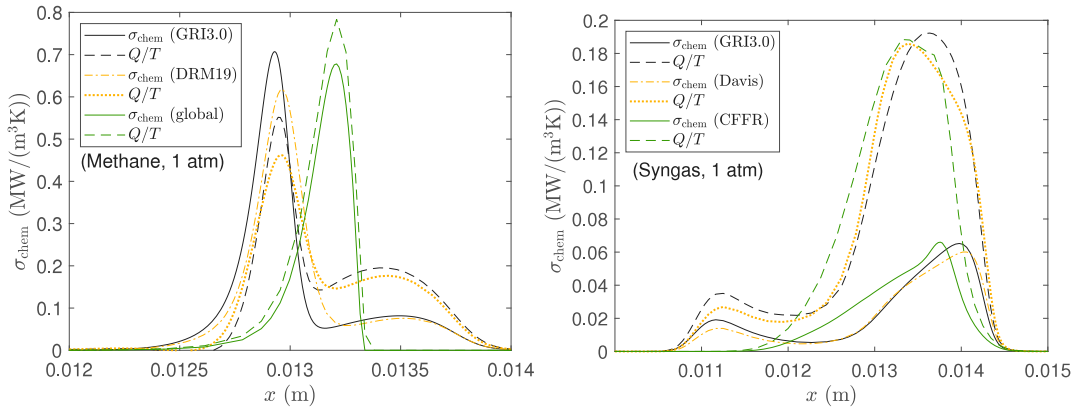

Fig. 15. Chemical reactions entropy generation rate along axis compared to a simplified model based on heat release rate from the same mechanism; methane–air and syngas–air with different mechanisms.

heat generation, temperature and amounts of certain species. When reactions are omitted, their contributions had to be compensated by modifications in remaining reactions. The extent of maintaining entropy generation (or not) can be seen as a side effect.

The reduced mechanisms inherit the defects and weaknesses of the full mechanism they are reduced from. Additional deficiencies can be introduced during the reduction process. Hence, for a reduced mechanism, results of the full mechanism can serve as a benchmark, both for entropy generation and other quantities.

Above, it was seen that temperature and major species were well represented by the reduced mechanisms, as expected. This also results in generally good predictions of entropy generation due to conduction by the reduced mechanisms when compared with the full mechanism. Furthermore, most reactions important for heat generation in the full mechanism were also important in the reduced mechanisms (Tables 2–3), although with some shift of weight.

Formulation of global mechanisms, with one or a few steps, gives few parameters to adapt and more compromises to be made. The focus is on heat release, temperature and major species, which gives rougher approximations. Nevertheless, these are the main input to calculations of entropy, which can be satisfactorily made when those quantities are well approximated.

5. Conclusions

Entropy generation in an opposed-flow laminar non-premixed flame has been investigated. Methane–air and syngas–air flames have been simulated with a global, reduced and full chemical mechanisms at three different pressures (1, 10 and 20 atm). Deviations from the full mechanism results by reduced and global mechanisms have been highlighted.

* The most important contribution to entropy generation is due to conductive heat transfer. Since the temperature is well predicted by all mechanisms, the conduction entropy generation is also well calculated. The global mechanisms give slightly steeper temperature gradients and hence, larger entropy generation.

* For syngas (all pressures) and for methane at elevated pressure, mass diffusion gives the second largest contribution to entropy generation. For methane the mass diffusion entropy generation is slightly lower for the reduced mechanism than for the full mechanism. For syngas, the reduced mechanism gives small deviations from the full mechanism. The global mechanisms, with only major species included, have larger deviations, reaching above 20% when integrated along the axis.

* For methane at atmospheric pressure, chemical reactions are the second largest contribution to entropy generation. Again, the reduced mechanism gives moderate deviations from the full mechanism, while the global mechanism predicts a thinner reaction zone with faster reaction, i.e. a narrower and higher spike in the entropy generation. Integrated along the axis, the chemical entropy production deviates considerable (more than 40%) from the global mechanism. Indeed, it is noted that for syngas–air at elevated pressures, the chemical contribution to entropy generation is quite modest (below 1%).

* When comparing contributions to heat release and entropy generation for individual reactions of the mechanisms, it is seen that the importance of each reaction can deviate considerably from the reduced to the full mechanism. The entropy generation for a particular reaction can be very different in the two mechanisms.

* Simplified entropy-generation models, either based on heat release rate, or by including conduction entropy generation only, do not give precise information on entropy generation. However, when used with care, they can give an indication on the location and magnitude of the entropy generation for methane/air non-premixed flames.

CRediT authorship contribution statement

Simon J. Lorentzen: Conceptualization, Methodology, Software, Validation, Investigation, Writing – review & editing, Visualization. **Ivar S. Ertesvåg:** Conceptualization, Methodology, Writing – original draft, Writing – review & editing, Supervision.

Declaration of competing interest

The authors declare that they have no known competing financial interests or personal relationships that could have appeared to influence the work reported in this paper.

Data availability

Data will be made available on request.

Acknowledgements

The authors appreciate discussions with Dr. Ning Guo at the same department.

This work was partly funded by the Norway Grants 2014-2021 via the National Centre for Research and Development of Poland. This article has been prepared within the frame of the project: “Negative CO2 emission gas power plant” - NOR/POLNORCCS/NEGATIVE-CO2-PP/0009/2019-00 which is co-financed by programme “Applied research” under the Norwegian Financial Mechanisms 2014-2021 POLNOR CCS 2019 - Development of CO2 capture solutions integrated in power and industry processes.

References

[1] Salimath PS, Ertesvåg IS. Local entropy generation and entropy fluxes of a transient flame during head-on quenching towards solid and hydrogen-permeable porous walls. Int J Hydrog Energy 2021;46:26616–30. http://dx.doi.org/10.1016/j.ijhydene.2021.05.142.

[2] Datta A. Entropy generation in a confined laminar diffusion flame. Combust Sci Tech 2000;159:39–56. http://dx.doi.org/10.1080/00102200008935776.

[3] Stanciu D, Isvoranu D, Marinescu M, Gogus Y. Second law analysis of diffusion flames. Int J Thermodyn 2001;4:1–18, URL:.

[4] Nishida K, Takagi T, Kinoshita S. Analysis of entropy generation and energy loss during combustion. Proc Combust Inst 2002;29:869–74. http://dx.doi.org/10.1016/S1540-7489(02)80111-0.

[5] Briones AM, Mukhopadhyay A, Aggarwal SK. Analysis of entropy generation in hydrogen-enriched methane-air propagating triple flames. Int J Hydrog Energy 2009;34:1074–83. http://dx.doi.org/10.1016/j.ijhydene.2008.09.103.

[6] Raghavan V, Gogos G, Babu V, Sundararajan T. Entropy generation during the quasi-steady burning of spherical fuel particles. Int J Therm Sci 2007;46:589–604. http://dx.doi.org/10.1016/j.ijthermalsci.2006.07.006.

[7] Pope DN, Raghavan V, Gogos G. Gas-phase entropy generation during transient methanol droplet combustion. Int J Therm Sci 2010;49:1288–302. http://dx.doi.org/10.1016/j.ijthermalsci.2010.02.012.

[8] Zhang Z, Lou C, Long Y, Kumfer BM. Thermodynamics second-law analysis of hydrocarbon diffusion flames: Effects of soot and temperature. Combust Flame 2021;234:111618. http://dx.doi.org/10.1016/j.combustflame.2021.111618.

[9] Yan H, Tang G, Wang C, Li L, Zhou Y, Zhang Z, Lou C. Thermodynamics irreversibilities analysis of oxy-fuel diffusion flames: The effect of oxygen concentration. Entropy 2022;24:205. http://dx.doi.org/10.3390/e24020205.

[10] Chen S, Han H, Liu Z, Li J, Zheng C. Analysis of entropy generation in non-premixed hydrogen versus heated air counter-flow combustion. Int J Hydrog Energy 2010;35:4736–46. http://dx.doi.org/10.1016/j.ijhydene.2010.02.113.

[11] Chen S, Liu Z, Liu J, Li J, Wang L, Zheng C. Analysis of entropy generation in hydrogen-enriched ultra-lean counter-flow methane-air non-premixed combustion. Int J Hydrog Energy 2010;35:12491–501. http://dx.doi.org/10.1016/j.ijhydene.2010.08.048.

[12] Liu Y, Chen S, Yang B, Liu K, Zheng C. First and second thermodynamic-law comparison of biogas MILD oxy-fuel combustion moderated by CO2 or H2O. Energy Convers Manage 2015;106:625–34. http://dx.doi.org/10.1016/j.enconman.2015.09.076.

[13] Lorentzen SJ. Understanding energy conversion in combustion - a detailed analysis of entropy production in flames (Master's thesis), Norway: NTNU Norwegian University of Science and Technology; 2021, URL: http://hdl.h{andl}e.net/11250/2787908.

[14] Kooshkbaghi M, Frouzakis CE, Boulouchos K, Karlin IV. Entropy production analysis for mechanism reduction. Combust Flame 2014;161:1507–15. http://dx.doi.org/10.1016/j.combustflame.2013.12.016.

[15] Kee RJ, Coltrin ME, Glarborg P, Zhu H. Chemically reacting flow: theory and practice. second ed.. Wiley; 2005.

[16] Bird BB, Stewart WE, Lightfoot EN. Transport phenomena. second ed.. New York: Wiley; 2002.

[17] Liu Y, Rogg B. Modelling of thermally radiating diffusion flames with detailed chemistry and transport. In: Heat transfer in radiating and combusting systems. Springer; 1991, p. 114–27.

[18] Haase R. Thermodynamics of irreversible processes. Reading, Massachusetts: Addison-Wesley; 1963.

[19] Smith GP, Golden DM, Frenklach M, Moriarty NW, Eiteneer B, Goldenberg M, Bowman CT, Hanson RK, Song S, Gardiner Jr W, Lissianski VV, Qin Z. http://me.berkeley.edu/gri_mech/, n.d. (Accessed on 2020-09-10).

[20] Kazakov A, Frenklach M. Reduced reaction sets based on gri-mech 1.2. 2020, http://combustion.berkeley.edu/drm/, n.d. (Accessed on 2020-09-10).

[21] Frenklach M, Wang H, Yu C-L, Goldenberg M, Bowman CT, Hanson RK, Davidson DF, Chang EJ, Smith GP, Golden DM, Gardiner WC, Lissianski V. http://combustion.berkeley.edu/gri-mech/new21/data/rxns_static.html, n.d. (Accessed on 2022-02-28).

[22] Westbrook CK, Dryer FL. Simplified reaction mechanisms for the oxidation of hydrocarbon fuels in flames. Combust Sci Tech 1981;27:31–43. http://dx.doi.org/10.1080/00102208108946970.

[23] Davis SG, Joshi AV, Wang H, Egolfopoulos F. An optimized kinetic model of H2/CO combustion. Proc Combust Inst 2005;30:1283–92. http://dx.doi.org/10.1016/j.proci.2004.08.252.

[24] Cuoci A, Frassoldati A, Faravelli T, Ranzi E. Accuracy and flexibility of simplified kinetic models for cfd applications. Combust Colloq 2009;1–6.

[25] Westbrook CK, Dryer FL. Chemical kinetic modeling of hydrocarbon combustion. Proc Combust Inst 1984;10:1–57. http://dx.doi.org/10.1016/0360-1285(84)90118-7.

[26] Goodwin DG, Speth RL, Moffat HK, Weber BW. Cantera: An object-oriented software toolkit for chemical kinetics, thermodynamics, and transport processes, https://www.cantera.org, version 2.4.0.

[27] McBride BJ, Zehe MJ, Gordon S. NASA Glenn coefficients for calculating thermodynamic properties of individual species. Technical Report NASA/TP-2002-211556, Cleveland, Ohio: Glenn Research Center; 2002.

[28] Kee RJ, Dixon-lewis G, Miller JA. A FORTRAN computer code package for the evaluation of gas-phase multicomponent transport properties. Technical report SAND86-8246, Livermore, California: Sandia National Lab.; 1986.

[29] Luo C, Moghtaderi B, Kennedy EM, Dlugogorski BZ. Three-dimensional numerical study on flames. Chem Prod Process Model 2009;4. http://dx.doi.org/10.2202/1934-2659.1378.

[30] Som S, Ramírez A, Hagerdorn J, Saveliev A, Aggarwal S. A numerical and experimental study of counterflow syngas flames at different pressures. Fuel 2008;87:319–34. http://dx.doi.org/10.1016/j.fuel.2007.05.023.

[31] Benekos S, Frouzakis CE, Giannakopoulos GK, Bolla M, Wright YM, Boulouchos K. Prechamber ignition: An exploratory 2-D DNS study of the effects of initial temperature and main chamber composition. Combust Flame 2020;215:10–27. http://dx.doi.org/10.1016/j.combustflame.2020.01.014.

[32] Yapıcı H, Kayataş N, Albayrak B, Başürk G. Numerical calculation of local entropy generation in a methane-air burner. Energy Convers Manage 2005;46:1885–919. http://dx.doi.org/10.1016/j.enconman.2004.09.007.

[33] Morsli S, Sabeur A, El Ganaoui M, Ramenah H. Computational simulation of entropy generation in a combustion chamber using a single burner. Entropy 2018;20. http://dx.doi.org/10.3390/e20120922.

[34] Saqr KM, Wahid MA. Entropy generation in turbulent swirl-stabilized flame: Effect of hydrogen enrichment. In: Advances in Thermofluids. Applied mechanics and materials, Vol. 388, Trans Tech Publications Ltd; 2013, p. 280–4. http://dx.doi.org/10.4028/www.scientific.net/AMM.388.280.

[35] Frenklach M, Wang H, Rabinowitz MJ. Optimization and analysis of large chemical kinetic mechanisms using the solution mapping method – combustion of methane. Prog Energy Combust Sci 1992;18:47–73. http://dx.doi.org/10.1016/0360-1285(92)90032-V.